Applied Physics Letters ARTICLE scitation.org/journal/apl

Bright electroluminescence in ambient conditions from WSe_2 p-n diodes using pulsed injection

Cite as: Appl. Phys. Lett. **115**, 011103 (2019); doi: 10.1063/1.5100306
Submitted: 16 April 2019 · Accepted: 10 June 2019 ·
Published Online: 1 July 2019

Kevin Han,[1,a)] Geun Ho Ahn,[1,2] Joy Cho,[1,2] Der-Hsien Lien,[1,2] Matin Amani,[1,2] Sujay B. Desai,[1,2] George Zhang,[1,2] Hyungjin Kim,[1,2] Niharika Gupta,[1,2] Ali Javey,[1,2] and Ming C. Wu[1]

AFFILIATIONS

[1]Electrical Engineering and Computer Sciences, University of California at Berkeley, Berkeley, California 94720, USA
[2]Materials Sciences Division, Lawrence Berkeley National Laboratory, Berkeley, California 94720, USA

[a)]Author to whom correspondence should be addressed: kyh@eecs.berkeley.edu

ABSTRACT

Transition metal dichalcogenide (TMDC) monolayers are promising materials for next-generation nanoscale optoelectronics, including high-speed light sources and detectors. However, most past reports on TMDC light-emitting diodes are limited to operation in high vacuum, while most applications require operation under ambient conditions. In this work, we study the time-resolved electroluminescence of monolayer WSe_2 p-n junctions under ambient conditions and identify the decay in current over time as the main issue preventing stable device operation. We show that pulsed voltage bias overcomes this issue and results in bright electroluminescence under ambient conditions. This is achieved in a simple single-gate structure, without the use of dual gates, heterostructures, or doping methods. Internal quantum efficiency of electroluminescence reaches ~1%, close to the photoluminescence quantum efficiency, indicating efficient exciton formation with injected carriers. Emission intensity is stable over hours of device operation. Finally, our device exhibits ~15 ns rise and fall times, the fastest direct modulation speed reported for TMDC light-emitting diodes.

Monolayer transition metal dichalcogenides (TMDCs) are a class of single-molecule-thick direct-bandgap semiconductors that show great potential for next-generation electronics[1–5] as well as optoelectronic devices such as light-emitting diodes (LEDs) and photodetectors.[6–13] Past works on TMDC LEDs have shown high electroluminescence (EL) quantum efficiencies of ~1%–5%.[6,7,14,15] However, these are generally reported under high-vacuum conditions, where environmental factors such as moisture and oxygen are partially avoided. On the other hand, most practical applications require operation under ambient conditions. A recent work on vertical light-emitting WS_2 tunneling structures showed sample degradation after only a few minutes of continuous operation in an ambient environment,[16] highlighting the importance of improving the stability under such conditions. In this work, we show that lateral-junction TMDC LEDs under ambient conditions exhibit fast exponential decay in light emission and current over a period of seconds, similar to past reports on current decay in TMDC field-effect transistors.[17,18] Inspired by a report on bright electroluminescence from pulsed TMDC capacitors,[13] we propose pulsed bias as a way to overcome this problem in light-emitting diodes, and show that it yields bright and stable EL from monolayer WSe_2 LEDs under ambient conditions. The EL quantum efficiency is ~1%, close to that of photoluminescence (PL). This implies that the EL efficiency in our devices is primarily limited not by charge carrier confinement, but by intrinsic material quality. In addition, time-resolved electroluminescence under pulsed injection reveals fast rise and fall times of ~15 ns, indicating strong potential for high-speed light modulation. Under pulsed bias, light emission is stable over hours. Our work is a key step toward realizing fast and efficient optical communication on the nanoscale using TMDC light emitters.

Our device design [Fig. 1(a)] is a back-gated WSe_2 FET structure operated as a p-n diode. The gate stack is either 50 nm SiO_2 on a p++ Si substrate, or 20 nm Al_2O_3 on a transparent ITO/glass substrate. Devices on both substrates showed bright light emission. WSe_2 was chosen due to its ambipolar nature, required for bipolar carrier injection. In general, most devices were ambipolar or slightly p-type in their I_d-V_g characteristics (supplementary material Figs. 1 and 7). Identical structures using monolayer MoS_2 showed only n-type I_d-V_g and no light emission (supplementary material Fig. 2). For diode operation, one contact is designated as the P contact with alternating the voltage between V_p and V_g, while the other (N) contact alternates between V_n and V_g [Fig. 1(b)]. Light is emitted only during the on period t_{on}. Figure 1(c) shows the EL spectrum of the device overlaid with the

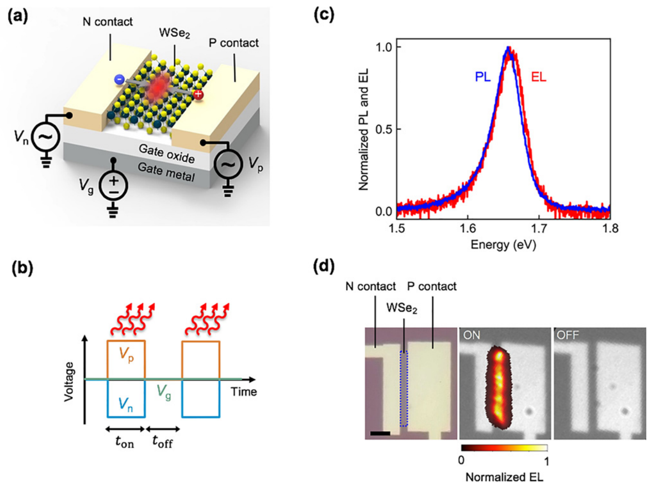

FIG. 1. Light emission from pulsed WSe_2 p-n diodes. (a) Device schematic. Contact/gate oxide/gate stack is either Ni (15 nm)/SiO_2 (50 nm)/Si or Ni (15 nm)/Al_2O_3 (20 nm)/ITO. (b) Schematic of voltage pulsing. Light is emitted when both $V_p > V_g$ and $V_n < V_g$, while during the off state $V_p = V_n = V_g$. (c) EL and PL spectra taken on the same device. (d) Spatial map of emission from an etched device. Left: optical micrograph. Scale bar is 5 μm. Middle: emission intensity during pulsed injection, overlaid on a CCD image. Emission occurs in the channel region between the two contacts. Right: device in the off state with no bias applied.

photoluminescence (PL) spectrum of the same device. The clear peak at ~1.65 eV shows that EL and PL are both due to the usual recombination of A excitons and confirms the monolayer nature of the flakes. PL quantum efficiency vs pump intensity shows a drop at high pump intensity due to exciton-exciton recombination, similar to past work[19] (supplementary material Fig. 3). Figure 1(d) shows the light emission overlaid on an image of the device, confirming emission comes from the channel region.

To illustrate the need for pulsed bias, we measure EL vs time and current vs time for both the DC (step) voltage and the pulsed voltage at 5 kHz. Bright emission is observed under both DC and pulsed biases. Note that the emission mechanism in our devices is clearly distinct from the pulsed light-emitting capacitors reported previously,[13] since continuous light emission is seen on a scale of ~seconds, as opposed to the ~10 ns pulses that occur only during voltage transitions. However, under DC bias, both emission and current rapidly decay by orders of magnitude within a few seconds [Figs. 2(a) and 2(b)]. Past reports on current decay in MoS_2 FETs show roughly comparable time constants ~10 s.[17,18] The ratio of light emission to current, which is proportional to the efficiency, remains roughly constant over time, showing that the decay in current is responsible for the decay in light emission. In contrast, pulsed bias yields extremely stable light emission and current over >1000 s [Figs. 2(c) and 2(d)]. Most devices under pulsed bias showed no decrease or a small decrease (<2×) in light emission in the first few minutes, then remained stable for the remaining duration of the applied bias, with the longest test performed being >3 h (supplementary material Fig. 4). The frequency response is shown in Fig. 2(e). Here, the emission intensity is defined as the average intensity over 10 s, starting 5 s after the pulsed bias is applied. Above ~1 kHz, the emission intensity is relatively stable with frequency, while below ~1 kHz, current decay causes EL to drop very quickly. However, note that the stability also depends on the duty cycle, which is fixed at 50% here. For a very low duty cycle ($t_{off} \gg t_{on}$), the emission intensity can still be stable at low frequencies ~0.1 Hz, i.e., a quasi-DC regime (supplementary material Figs. 10 and 11), indicating no permanent device degradation at DC bias (see the supplementary material for details on the causes of current decay).

Next, we study the emission characteristics under varying bias to extract the optimal bias conditions. The relative injection level of electrons and holes, and thus the exciton formation efficiency, depends on the voltages ($V_p - V_g$) and ($V_n - V_g$) applied to the contacts. If $|V_p - V_g| \gg |V_n - V_g|$, holes will be predominantly injected and will simply diffuse across the channel to the opposite contact without forming excitons, and vice versa for $|V_p - V_g| \ll |V_n - V_g|$ [Fig. 3(a)]. We determine the optimal bias condition by keeping ($V_p - V_n$) constant and sweeping V_g from V_n to V_p while tracking the EL and current. Figure 3(b) shows the EL intensity vs gate voltage along with the current and EL efficiencies, where V_p and V_n are fixed at $V_p = 5$ V and $V_g = -5$ V. Each point corresponds to one on period $t_{on} = 0.5$ s, and the current and emission intensity are defined as the time-average during the on period. An off time of $t_{off} = 10$ s is used to recover the device between pulses (supplementary material). The brightest

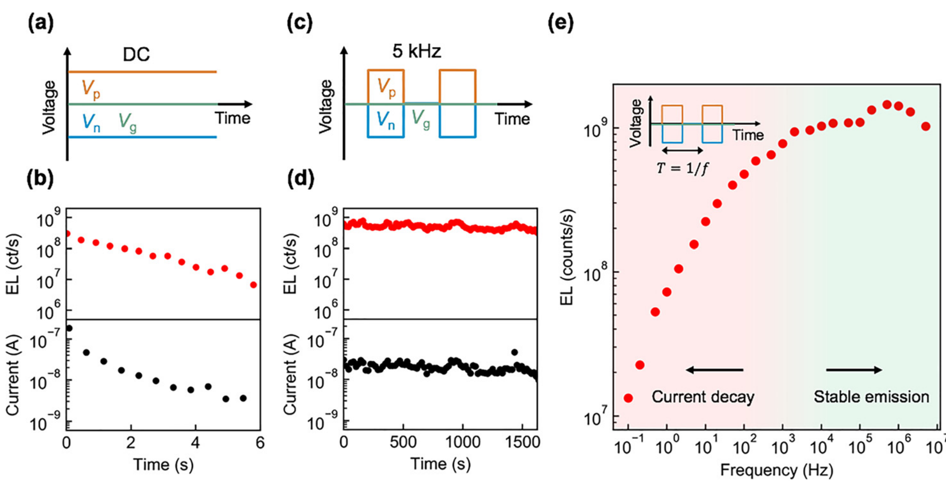

FIG. 2. Light emission and current for DC and pulsed biases. (a) Schematic of the DC voltage bias. (b) Light emission and current over time for the DC voltage of $V_p = -V_n = 4$ V, with $V_g = 0$ V. (c) Schematic of the pulsed voltage bias, using a square wave with 50% duty cycle. (d) Light emission and current over time for the pulsed voltage with $V_p = -V_n = 4$ V, with $V_g = 0$ V. Note the different time scales for (b) and (d). (e) Frequency response with $V_p = -V_n = 4.5$ V, recorded with a different device from (b) and (d).

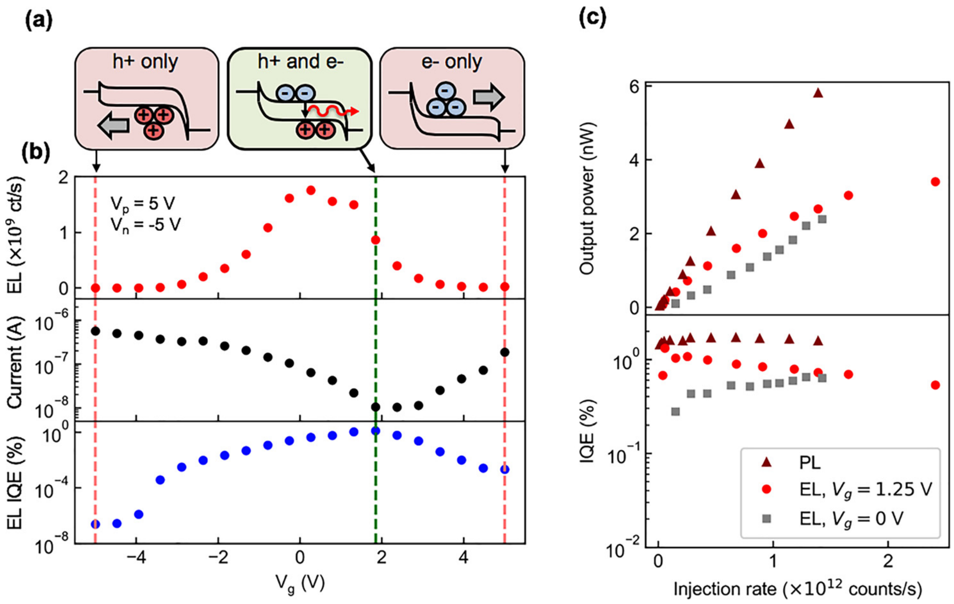

FIG. 3. L-I-V characteristics and optimal bias conditions. (a) Schematic of carrier injection regimes with varying gate voltage and fixed V_p and V_n. (b) EL intensity, current, and EL IQE vs gate voltage V_g, for constant $V_p = -V_n = 5\,\text{V}$. (c) Output power and IQE vs carrier injection rate for PL and EL. EL is recorded under near-optimal bias conditions extracted from V_g sweep ($V_g = 1.25\,\text{V}$), as well as from $V_g = 0\,\text{V}$ for comparison.

emission occurs near $V_g = 0\,\text{V}$, where both holes and electrons are injected. The minimum current point at $V_g \approx 1.8\,\text{V}$ corresponds to the most bipolar injection and coincides with the highest internal quantum efficiency (IQE) of ∼1%. $|V_p - V_g| < |V_n - V_g|$ at this point, indicating slightly p-type characteristics typical for monolayer WSe_2. We obtain an L-I curve under optimal bias conditions by first setting $V_g = 1.25$ V, approximately the point of maximum efficiency above which the current is also not too low. Then, we increase the source-drain bias, while keeping $|V_p - V_g|/|V_n - V_g|$ constant at ∼0.6. For comparison, we also take an L-I curve with $V_g = 0\,\text{V}$ (i.e., equal $|V_p - V_g|$ and $|V_n - V_g|$). L-I and IQE are plotted in Fig. 3(c), along with the corresponding PL L-L curves. PL shows a roughly constant IQE of ∼1.6%, while EL at an optimal bias shows a peak of ∼1.3% at low current and decreases slightly at higher currents, possibly due to variation in optimal bias conditions with voltage. In contrast, EL at equal P and N biases is low (∼0.3%) at low current and stays below ∼0.8% throughout.

Next, we study the modulation speed of the device by performing time-resolved measurements using time-correlated single-photon counting (TCSPC). Supplementary material Fig. 5 shows the measurement setup and Fig. 4 shows time-resolved electroluminescence at 1 MHz, together with the P and N voltage pulses measured on an oscilloscope. Emission occurs only when both P and N voltages are applied, confirming bipolar carrier injection. The emission intensity is nearly constant during the entire P/N voltage overlap period. The rise and fall times shown in the inset are ∼12 ns and ∼18 ns, respectively. We note that this rise/fall time is ∼20× faster than monolayer LEDs using vertical tunnel injection heterostructures,[20] which is due to the lower capacitance of the lateral injection scheme used here. Tunnel junctions require extremely thin oxide layers (∼1–2 nm) for current injection, leading to high capacitance. The rise and fall times are limited by the function generator used, as can be seen in the voltage pulses measured on the oscilloscope (Fig. 4, top). Therefore, the actual device speed is likely faster, ultimately limited by the intrinsic radiative lifetime of ∼few nanoseconds.[21]

In this work, we have shown that the hysteresis and current decay commonly seen in TMDC transistors also play an important role in light-emitting diodes. Pulsed injection is an effective way to circumvent this issue, yielding bright and stable EL using a simple back-gated FET structure, with efficiency near that of PL. We show how to extract the optimal bias conditions for efficient bipolar injection and study the high frequency behavior of light emission. A fast ∼15 ns rise/fall time is observed, indicating strong potential for high speed light modulation. Pulsed emission is stable over hours of operation. Further

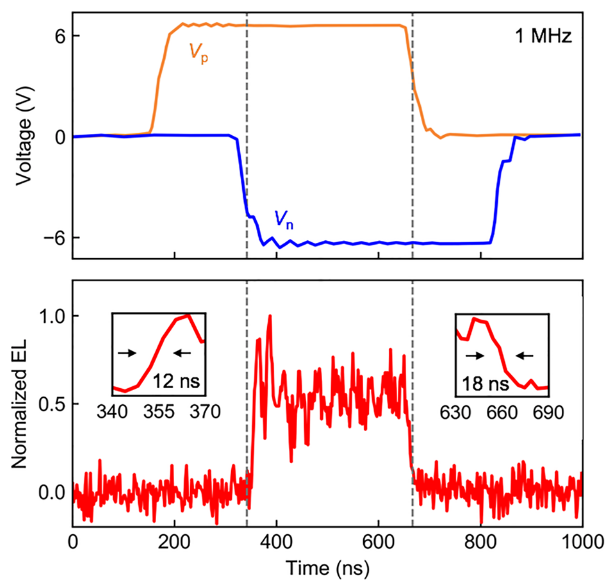

FIG. 4. Time-resolved light emission. Top panel: voltage pulses measured on an oscilloscope. Bottom panel: time-resolved EL. Left inset: close-up of EL rise time. Right inset: close-up of EL fall time.

improvements in efficiency will come from contact optimization to enable lower voltage operation, as well as advances in chemical vapor deposition (CVD) growth to improve intrinsic material quality. Higher speed can be obtained by coupling to an optical cavity to enhance spontaneous emission rate.[20,22–24]

See the supplementary material for additional tests on the causes of current decay, description of IQE calculation, and further device and material characterization data.

Device fabrication and characterization were funded by the Center for Energy Efficient Electronics Science through a grant from the National Science Foundation (NSF Award No. ECCS-0939514). K.H. was supported by the Department of Defense (DoD) through the National Defense Science & Engineering Graduate Fellowship (NDSEG) Program. WSe_2 growth was supported by the Electronic Materials Program funded by the Director, Office of Science, Office of Basic Energy Sciences, Materials Sciences and Engineering Division of the U.S. Department of Energy, under Contract No. DE-AC02-05Ch11231.

REFERENCES

[1]H. Fang, S. Chuang, T. C. Chang, K. Takei, T. Takahashi, and A. Javey, Nano Lett. **12**, 3788 (2012).
[2]S. Das, H.-Y. Chen, A. V. Penumatcha, and J. Appenzeller, Nano Lett. **13**, 100 (2013).
[3]S. Bhattacharjee, K. L. Ganapathi, S. Mohan, and N. Bhat, Appl. Phys. Lett. **111**, 163501 (2017).
[4]L. Xie, M. Liao, S. Wang, H. Yu, L. Du, J. Tang, J. Zhao, J. Zhang, P. Chen, X. Lu, G. Wang, G. Xie, R. Yang, D. Shi, and G. Zhang, Adv. Mater. **29**, 1702522 (2017).
[5]B. Radisavljevic, A. Radenovic, J. Brivio, V. Giacometti, and A. Kis, Nat. Nanotechnol. **6**, 147 (2011).
[6]B. W. H. Baugher, H. O. H. Churchill, Y. Yang, and P. Jarillo-Herrero, Nat. Nanotechnol. **9**, 262 (2014).
[7]A. Pospischil, M. M. Furchi, and T. Mueller, Nat. Nanotechnol. **9**, 257 (2014).
[8]J. S. Ross, P. Klement, A. M. Jones, N. J. Ghimire, J. Yan, D. G. Mandrus, T. Taniguchi, K. Watanabe, K. Kitamura, W. Yao, D. H. Cobden, and X. Xu, Nat. Nanotechnol. **9**, 268 (2014).
[9]J. Binder, F. Withers, M. R. Molas, C. Faugeras, K. Nogajewski, K. Watanabe, T. Taniguchi, A. Kozikov, A. K. Geim, K. S. Novoselov, and M. Potemski, Nano Lett. **17**, 1425 (2017).
[10]J. S. Ross, P. Rivera, J. Schaibley, E. Lee-Wong, H. Yu, T. Taniguchi, K. Watanabe, J. Yan, D. Mandrus, D. Cobden, W. Yao, and X. Xu, Nano Lett. **17**, 638 (2017).
[11]A. E. Yore, K. K. H. Smithe, S. Jha, K. Ray, E. Pop, and A. K. M. Newaz, Appl. Phys. Lett. **111**, 043110 (2017).
[12]V. Dhyani and S. Das, Sci. Rep. **7**, 44243 (2017).
[13]D.-H. Lien, M. Amani, S. B. Desai, G. H. Ahn, K. Han, J.-H. He, J. W. Ager, M. C. Wu, and A. Javey, Nat. Commun. **9**, 1229 (2018).
[14]F. Withers, O. Del Pozo-Zamudio, S. Schwarz, S. Dufferwiel, P. M. Walker, T. Godde, A. P. Rooney, A. Gholinia, C. R. Woods, P. Blake, S. J. Haigh, K. Watanabe, T. Taniguchi, I. L. Aleiner, A. K. Geim, V. I. Fal'ko, A. I. Tartakovskii, and K. S. Novoselov, Nano Lett. **15**, 8223 (2015).
[15]F. Withers, O. Del Pozo-Zamudio, A. Mishchenko, A. P. Rooney, A. Gholinia, K. Watanabe, T. Taniguchi, S. J. Haigh, A. K. Geim, A. I. Tartakovskii, and K. S. Novoselov, Nat. Mater. **14**, 301 (2015).
[16]Y. Sheng, T. Chen, Y. Lu, R.-J. Chang, S. Sinha, and J. H. Warner, ACS Nano **13**, 4530 (2019).
[17]D. J. Late, B. Liu, H. S. S. R. Matte, V. P. Dravid, and C. N. R. Rao, ACS Nano **6**, 5635 (2012).
[18]A. Di Bartolomeo, L. Genovese, F. Giubileo, L. Iemmo, G. Luongo, T. Foller, and M. Schleberger, 2D Mater. **5**, 015014 (2017).
[19]M. Amani, P. Taheri, R. Addou, G. H. Ahn, D. Kiriya, D.-H. Lien, J. W. Ager, R. M. Wallace, and A. Javey, Nano Lett. **16**, 2786 (2016).
[20]C.-H. Liu, G. Clark, T. Fryett, S. Wu, J. Zheng, F. Hatami, X. Xu, and A. Majumdar, Nano Lett. **17**, 200 (2017).
[21]M. Palummo, M. Bernardi, and J. C. Grossman, Nano Lett. **15**, 2794 (2015).
[22]Z. Wang, Z. Dong, Y. Gu, Y.-H. Chang, L. Zhang, L.-J. Li, W. Zhao, G. Eda, W. Zhang, G. Grinblat, S. A. Maier, J. K. W. Yang, C.-W. Qiu, and A. T. S. Wee, Nat. Commun. **7**, 11283 (2016).
[23]G. M. Akselrod, T. Ming, C. Argyropoulos, T. B. Hoang, Y. Lin, X. Ling, D. R. Smith, J. Kong, and M. H. Mikkelsen, Nano Lett. **15**, 3578 (2015).
[24]M. Eggleston, S. Desai, K. Messer, S. Madhvapathy, J. Xiao, X. Zhang, E. Yablonovitch, A. Javey, and M. C. Wu, in *CLEO 2015 Paper FTu1E5* (Optical Society of America, 2015), p. FTu1E.5.